User-Centric Cell-Free Massive MIMO System for Indoor Industrial Networks

Haijun Zhang, *Senior Member, IEEE*, Renwei Su, Yongxu Zhu, *Senior Member, IEEE*, Keping Long, *Senior Member, IEEE*, and George K. Karagiannidis, *Fellow, IEEE*

***Abstract*—The cell-free massive multiple-input multiple-output (CFmMIMO) aims to provide uniform quality of service (QoS) for all users, and can be used in small-area scenarios such as indoor industrial networks. This paper studies the CFmMIMO system for indoor industrial scenarios. Firstly, an access point (AP) grouping based hierarchical network topology is proposed. Based on this, we propose an effective AP selection method. To reduce pilot contamination, a pilot assignment scheme based on inspection robot (IR) location is proposed. Considering the high reliability requirement of industrial data transmission, the power control and backhaul combining are jointly optimized to maximize the minimum signal to interference plus noise ratio (SINR). The scalability of the proposed CFmMIMO system is analyzed, and a scalable power control method is proposed. The simulations demonstrate the effectiveness of the AP selection method, pilot assignment scheme, and the joint optimization algorithm for power control and backhaul combining. Moreover, the impact of network scale and network load on system performance is evaluated and analyzed in the simulations.**

***Index Terms*—Cell-free massive MIMO, indoor industrial networks, pilot assignment, power control, system scalability.**

I. Introduction

Due to signal attenuation and intercell interference, it is difficult for users at the cell edge to obtain the same quality of service (QoS) as users at the cell center in current cellular networks [1]. The centralized massive multiple-input multiple-output (MIMO) can increase channel gain and enhance coverage [2]–[4], but it still faces the above-mentioned problem. In the distributed antenna system (DAS) [5], the traditional single base station configured with centralized massive antennas is transformed into several multi-antenna or single-antenna access points (APs) scattered in the cell. Although DAS can improve the QoS of edge users, each user can only be served by APs in the cell to which it is attached, and intercell interference is still severe due to lack of cooperation of APs in different cells. The cell-free massive MIMO (CFmMIMO), which aims to provide users with uniform QoS [1], [6], is considered as a potential technology to solve this problem. In a cell-free network, a large number of APs are deployed in the target area without dividing these APs into several cells. Therefore, APs that have a greater impact on a user, or even all APs in the area, can cooperate to serve this user, so that each user can obtain almost uniform QoS.

Ngo et al. in [1] proposed a classic CFmMIMO architecture, using large numbers of APs to cover the target area, and all APs serve all users simultaneously. In such an architecture, each user is served by all APs at the same time, resulting in high load on each AP and large backhaul overhead. After that, a CFmMIMO architecture based on user-centric approach was proposed in [7], in which each AP only serves a few users with the best channel conditions. In such user-centric network, users in the coverage area have equal status to select the serving APs that may provide the best service [6]. From the perspective of each user, all APs serving it constitute a virtual cell [5], [7]. Compared with the classical architecture, the user-centric CFmMIMO has obvious advantages and is more realistic [8]. First, each AP only serves a subset of users, which can reduce the load and energy consumption of each AP. In addition, the data transmitted from the APs to the CPU will be less, which can significantly reduce the backhaul overhead [7]. More importantly, when applying a reasonable AP selection scheme, users can obtain better QoS [7] or higher energy efficiency [9] compared to the classic architecture. Therefore, the user-centric CFmMIMO is gradually recognized and studied [6]–[10].

Many studies have been carried out on CFmMIMO power control [1], [11], [12], beamforming [12]–[14], user grouping [15]–[17], pilot assignment [18], [19], AP selection [9], [20], backhaul combining [21], [22], system scalability [6], [8], [23], etc., so that the system performance is continuously improved. Although the CFmMIMO has broad research and application prospects [6], it is still not practical to completely replace the classic cellular networks. Due to the wide coverage of the cellular networks, it is obviously difficult and costly to use large numbers of APs to obtain the same coverage. However, in wireless networks for hotspot areas where the coverage area is not too large, such as indoor industrial networks, CFmMIMO can be practically applied.

With the advancement of wireless communication technology and Internet of Things (IoT) technology, various industrial services are developing towards digitization [24]–[26]. The

This work is supported in part by the National Key R&D Program of China (2021YFB2900801), the National Natural Science Foundation of China (62225103), Beijing Natural Science Foundation (L212004), and China University Industry-University-Research Collaborative Innovation Fund (2021FNA05001). (*Corresponding author: Haijun Zhang.*)

H. Zhang, R. Su, and K. Long are with Beijing Engineering and Technology Research Center for Convergence Networks and Ubiquitous Services, University of Science and Technology Beijing, Beijing, China, 100083 (e-mail:haijunzhang@ieee.org, surenwei@xs.ustb.edu.cn, longkeping@ustb.edu.cn).

Y. Zhu is with the Division of Computer Science and Informatics, London South Bank University, London SE1 0AA, U.K. (e-mail: yongxu.zhu@lsbu.ac.uk).

G. K. Karagiannidis is with the Aristotle University of Thessaloniki, 54124 Thessaloniki, Greece (e-mail: geokarag@auth.gr).

application of CFmMIMO in industrial wireless networks has gained attention. The work in [27] compared the performance of different transmission modes in industrial scenarios, and selected the signal to interference plus noise ratio (SINR) and achievable rate of the actuators as performance metrics, indicating that the cell-free transmission mode can improve the reliability and delay of transmission. The serving APs of each user are determined according to the distance in the user-centric cell-free IoT network proposed in [28], and device activity detection method and channel estimation scheme in cell-free IoT with massive connectivity were also studied. The authors in [22] proposed an uplink cell-free Industrial IoT architecture, and jointly optimized power control and backhaul combining to improve the average success ratio of data transmission. The energy efficiency of IoT based on CFmMIMO was concerned by [29], and the max-min uplink power control method was adopted. Most of the studies did not propose a specific network topology [22], [27]–[29], but simply adopted the star topology. All APs are directly connected to the CPU by wire under such a topology, which will consume a lot of cables and cause high CPU load, so the star topology is not easy to be practically deployed in industrial scenarios. In terms of channel modeling, some crucial issues such as the unique channel environment and the mobility of some devices in industrial scenarios have not been considered. Moreover, as a very critical point in practical applications, the scalability of CFmMIMO system has not been fully analyzed and effectively guaranteed, especially the scalability of power control methods. Therefore, the CFmMIMO system for industrial scenarios needs to be studied more comprehensively.

This paper studies the CFmMIMO system for indoor industrial networks. In order to enable CFmMIMO systems in industrial scenarios to have superior performance, the network topology should be practical and feasible, and the reliability of data transmission needs to be guaranteed through operations such as pilot assignment and power control. In addition, the scalability of the system should also be considered. Considering an indoor industrial scenario, intelligent inspection robots (IRs) can check the operation status of the equipment and warn of the equipment malfunction, which requires reliable data transmission. Based on proposed novel network topology and channel model, this paper studies the CFmMIMO system for the uplink communication of the IRs, including AP selection, pilot assignment, power control, backhaul combining, and system scalability. The main contributions of this paper are as follows:

- An easy-to-deploy hierarchical network topology based on AP grouping is proposed for the CFmMIMO system. In the channel model, the mobility of the IRs and large numbers of scattering paths in indoor industrial scenarios are considered.
- User-centric mode is adopted in the cell-free industrial wireless network, so an AP selection method based on line-of-sight (LoS) path gain or large-scale fading (LSF) coefficient is proposed. In addition, we propose a pilot assignment scheme based on IR location to reduce pilot contamination effectively.

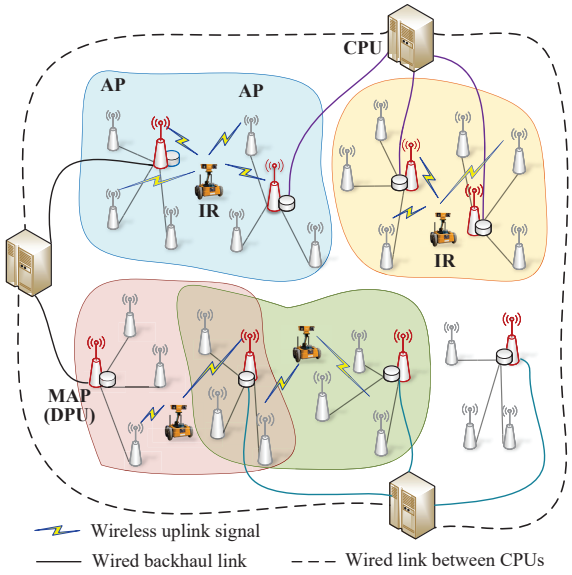

Fig. 1. CFmMIMO based indoor industrial networks.

- Considering the high reliability requirement of industrial data transmission, and taking maximizing the minimum SINR as the optimization objective, an improved bisection based joint optimization algorithm for power control and backhaul combining is proposed.
- The scalability of the proposed CFmMIMO system for indoor industrial networks is comprehensively analyzed. A distributed power control method is introduced, based on which a scalable power control method is proposed to further enhance the scalability of the system.

The rest of the paper is organized as follows. The system model and channel estimation are introduced in Section II. In Section III the uplink signal transmission is described in detail. Section IV introduces the proposed AP selection method and pilot assignment scheme. The joint optimization algorithm for power control and backhaul combining is proposed in Section V. In Section VI, the scalability of the proposed CFmMIMO system is analyzed. Simulations and discussions are provided in Section VII. This paper is concluded in Section VIII.

II. System Model and Channel Estimation

A. System Model

An indoor industrial scenario as shown in Fig. 1 is considered, in which K single-antenna IRs and M multi-antenna APs are deployed. Each AP is equipped with N antennas, and $MN \gg K$. Let m and k denote the indexes of the mth AP and the kth IR, respectively. Additionally, several central processing units (CPUs) connected to each other are also deployed [8], which means that these CPUs can cooperate to complete tasks.

All APs are divided into G AP groups (APGs) according to the proximity principle in terms of distance, which can be easily implemented in realistic scenarios. Let g denote the index of the gth APG. The set of APs in the gth APG is

represented as $\mathcal{A}(g)$. It is assumed that the number of APs in each APG is equal, which is $\frac{M}{G} \in \mathbb{N}$. Moreover, each IR is served by all APs from G_{sub} APGs, and $G_{sub} < G$. Then the number of APs serving each IR is $J = \frac{M}{G} G_{sub}$.

There is one AP in each APG as the main AP (MAP) with a distributed processing unit (DPU), which can processe part of the computing tasks in the AP selection, backhaul combining and power control stages. A hierarchical connection from APs to MAPs, and then from MAPs to CPUs is adopted. Other APs in each APG are connected to the MAP in that APG, then each MAP is connected to one of the CPUs. The wired links between APs and MAPs, and between MAPs and CPUs are called backhaul links.

The bandwidth of the system is B, and all IRs can use the full bandwidth to transmit data. The time division duplex mode is adopted in the system. There are τ_c samples in each coherence interval, of which τ_p samples are used for uplink training. Additionally, τ_u samples are used for uplink transmission, and the number of samples used for downlink transmission is $\tau_d = \tau_c - \tau_p - \tau_u$.

Considering the complex environment in the indoor industrial scenario, the uplink channel from IR k to AP m is expressed as [30]

$$\mathbf{h}_{k,m} = e^{j\theta_{k,m}} \bar{\mathbf{h}}_{k,m} + \tilde{\mathbf{h}}_{k,m}, \tag{1}$$

where $e^{j\theta_{k,m}} \bar{\mathbf{h}}_{k,m} \in \mathbb{C}^N$ represents the LoS component, and $\tilde{\mathbf{h}}_{k,m} \in \mathbb{C}^N$ represents the non-line-of-sight (NLoS) component. Due to the mobility of IRs, the LoS path between IR k and AP m has an unknown phase shift $\theta_{k,m}$ [31]. It is assumed that $\theta_{k,m}$ is uniformly distributed in $[0, 2\pi)$ for $k = 1, \cdots K$ and $m = 1, \cdots M$. Additionally, considering the influence of IRs mobility on a large number of scattering paths, the NLoS component is modeled as a complex Gaussian distribution [30], namely $\tilde{\mathbf{h}}_{k,m} \sim \mathcal{CN}(0_N, \beta_{k,m}\mathbf{I}_N)$, where $\beta_{k,m}$ is LSF coefficient. $\bar{\mathbf{h}}_{k,m}$ and $\beta_{k,m}$ represent the long-term channel state, so it is assumed that they are known [30]. The antennas of each AP are deployed as uniform linear array [2], so each element in $\bar{\mathbf{h}}_{k,m} = \left[\bar{h}_{km,1}, \bar{h}_{km,2}, \cdots, \bar{h}_{km,N}\right]^T$ represents the state of the LoS path between IR k and each antenna of AP m. Then $\left|\bar{h}_{km,n}\right|^2$ represents the corresponding path gain. $\left|\bar{h}_{km,n}\right|^2$ is equal for $n = 1, \cdots, N$, because the different elements in $\bar{\mathbf{h}}_{k,m}$ only differ in phase. Let $\alpha_{k,m} \triangleq |h_{km,n}|^2$ denote the LoS path gain between IR k and AP m, which is not related to the value of n.

B. Channel Estimation

Since each AP only serves part of the IRs, each AP only needs to estimate the corresponding channel state. τ_p mutually orthogonal pilots are used for channel estimation, and $\tau_p < K$. The pilot assigned to IR k is expressed as $\boldsymbol{\varphi}_k$, and $\|\boldsymbol{\varphi}_k\|^2 = \tau_p$. Let $\mathcal{P}(k)$ denote the set of IRs using the same pilot as IR k. At the stage of uplink training, the total pilot signal received by AP m is expressed as

$$\mathbf{Y}_m = \sum_{k=1}^{K} \sqrt{p_p} \mathbf{h}_{k,m} \boldsymbol{\varphi}_k^T + \mathbf{N}_m, \tag{2}$$

where p_p is the pilot signal transmit power. $\mathbf{N}_m$ is the additive noise matrix, all elements of which are independent and identically distributed (i.i.d.) $\mathcal{CN}\left(0, \sigma^2\right)$ random variables (RVs).

The projection of $\mathbf{Y}_m$ onto $\boldsymbol{\varphi}_k^*$ can be used as the sufficient statistics for the estimation of $\mathbf{h}_{k,m}$ [1], [30], namely

$$\mathbf{y}_{k,m} = \frac{\mathbf{Y}_m \boldsymbol{\varphi}_k^*}{\sqrt{\tau_p}} = \sqrt{\tau_p p_p} \sum_{k' \in \mathcal{P}(k)} \mathbf{h}_{k',m} + \mathbf{n}_{k,m}, \tag{3}$$

where

$$\mathbf{n}_{k,m} = \frac{\mathbf{N}_m \boldsymbol{\varphi}_k^*}{\sqrt{\tau_p}}. \tag{4}$$

The linear minimum mean-squared error (LMMSE) channel estimation of $\mathbf{h}_{k,m}$ is

$$\hat{\mathbf{h}}_{k,m} = \sqrt{\tau_p p_p} \mathbf{R}_{k,m} \boldsymbol{\Phi}_{k,m}^{-1} \mathbf{y}_{k,m}, \tag{5}$$

where

$$\mathbf{R}_{k,m} \triangleq \mathbb{E}\left\{\mathbf{h}_{k,m} \mathbf{h}_{k,m}^H\right\} = \bar{\mathbf{h}}_{k,m} \bar{\mathbf{h}}_{k,m}^H + \beta_{k,m} \mathbf{I}_N, \tag{6}$$

$$\begin{aligned} \boldsymbol{\Phi}_{k,m} &\triangleq \mathbb{E}\left\{\mathbf{y}_{k,m} \mathbf{y}_{k,m}^H\right\} \\ &= \tau_p p_p \sum_{i \in P_k} \left(\bar{\mathbf{h}}_{i,m} \bar{\mathbf{h}}_{i,m}^H + \beta_{i,m} \mathbf{I}_N\right) + \sigma^2 \mathbf{I}_N \end{aligned}. \tag{7}$$

Moreover, the covariance matrices of $\hat{\mathbf{h}}_{k,m}$ can be expressed as

$$\hat{\mathbf{R}}_{k,m} \triangleq \mathbb{E}\left\{\hat{\mathbf{h}}_{k,m} \hat{\mathbf{h}}_{k,m}^H\right\} = \tau_p p_p \mathbf{R}_{k,m} \boldsymbol{\Phi}_{k,m}^{-1} \mathbf{R}_{k,m}. \tag{8}$$

TABLE I
NOTATIONS USED IN THIS PAPER

Notations	Explanations
M	Number of APs
K	Number of IRs
B	Bandwidth of the system
G	Number of APGs
m	Index of the mth AP
k	Index of the kth IR
g	Index of the gth APG
$\mathcal{A}(g)$	Set of APs in the gth APG
G_{sub}	Number of APGs serving each IR
J	Number of APs serving each IR
τ_c	Number of samples in each coherence interval
τ_p	Number of samples used for uplink training
τ_u	Number of samples used for uplink transmission
$\mathbf{h}_{k,m}$	Uplink channel state
$\alpha_{k,m}$	LoS path gain
$\beta_{k,m}$	LSF coefficient
p_p	Pilot signal transmit power
p_u	Maximum uplink signal transmit power
φ_k	Pilot assigned to IR k
$\mathcal{P}(k)$	Set of IRs using the same pilot as IR k
$\mathcal{G}(k)$	Set of APGs serving IR k
$\mathcal{M}(k)$	Set of APs serving IR k
$M_k(j)$	Index of jth AP in $\mathcal{M}(k)$
η_k	Signal transmit power of IR k
$\mathbf{w}_k$	Backhaul combining coefficient vector for IR k

III. Uplink Data Transmission

In the indoor industrial scenario, each IR needs to upload the data collected during its inspection. We denote $\mathcal{G}(k)$ as the set of APGs serving IR k, which includes G_{sub} APGs. Let $\mathcal{M}(k)$ denote the set of APs serving IR k, include J APs from these G_{sub} APGs. The indexes of the corresponding APs are $M_k(1), M_k(2), \cdots, M_k(J)$, namely $\mathcal{M}(k) = \{M_k(1), M_k(2), \cdots, M_k(J)\}$. Let s_k denote the signal transmitted by IR k, then the received signal of AP m is

$$\mathbf{r}_m = \sum_{k=1}^{K} \sqrt{\eta_k}\mathbf{h}_{k,m} s_k + \mathbf{n}_m, \tag{9}$$

where η_k is the signal transmit power of IR k. $\mathbf{n}_m$ is additive noise vector, all elements of which are i.i.d. $\mathcal{CN}\left(0, \sigma^2\right)$ RVs.

If $m \in \mathcal{M}(k)$, AP m performs maximum ratio (MR) decoding to detect the symbol from IR k. The decoded signal of AP m is expressed as

$$\hat{r}_{k,m} = \hat{\mathbf{h}}_{k,m}^H \mathbf{r}_m. \tag{10}$$

After MR decoding, the DPU of each APG combines the MR decoded signals from the APs in this APG. Then MAPs transmit the combined signal to the CPU. Therefore, the combined signal received by the CPU is [31]

$$\hat{s}_k = \sum_{m \in \mathcal{M}(k)} w_{k,m}^* \hat{r}_{k,m}, \tag{11}$$

where $\{w_{k,m}\}$ is the set of weighted coefficients for the detection of the symbol from IR k. The above-mentioned backhaul combining method allocates the computing tasks to the DPUs, which can reduce the computing load of the CPU.

It is assumed that all CPUs only have channel statistics knowledge, which avoids the sharing of channel state information (CSI) in the network and reduces the requirement for backhaul [1], [30], [31]. Then $\hat{s}_k$ can be rewritten as

$$\hat{s}_k = DS_k s_k + BU_k s_k + \sum_{k' \neq k} UI_{k,k'} s_{k'} + \hat{n}_k, \tag{12}$$

where

$$DS_k = \sqrt{\eta_k} \sum_{m \in \mathcal{M}(k)} w_{k,m}^* \mathbb{E}\left\{\hat{\mathbf{h}}_{k,m}^H \mathbf{h}_{k,m}\right\}, \tag{13}$$

$$BU_k = \sqrt{\eta_k} \sum_{m \in \mathcal{M}(k)} w_{k,m}^* \left(\hat{\mathbf{h}}_{k,m}^H \mathbf{h}_{k,m} - \mathbb{E}\left\{\hat{\mathbf{h}}_{k,m}^H \mathbf{h}_{k,m}\right\}\right), \tag{14}$$

$$UI_{kk'} = \sqrt{\eta_{k'}} \sum_{m \in \mathcal{M}(k)} w_{k,m}^* \hat{\mathbf{h}}_{k,m}^H \mathbf{h}_{k',m}, \tag{15}$$

$$\hat{n}_k = \sum_{m \in \mathcal{M}(k)} w_{k,m}^* \hat{\mathbf{h}}_{k,m}^H \mathbf{n}_m. \tag{16}$$

DS_k and BU_k represent the strength of the desired signal (DS) and the beamforming gain uncertainty (BU), respectively. $UI_{kk'}$ denotes the interference caused by IR k' [1]. Then a lower bound on the uplink SINR for IR k is given by [1], [30]

$$SINR_k = \frac{|DS_k|^2}{\mathbb{E}\left\{|BU_k|^2\right\} + \sum\limits_{k' \neq k} \mathbb{E}\left\{|UI_{k,k'}|^2\right\} + \mathbb{E}\left\{|\hat{n}_k|^2\right\}}. \tag{17}$$

Some vectors and matrices are defined as follows:

$$\mathbf{w}_k \in \mathbb{C}^J, w_k^j \triangleq w_{k,M_k(j)}, \tag{18}$$

$$\mathbf{b}_k \in \mathbb{C}^J, b_k^j \triangleq \mathbb{E}\left\{\hat{\mathbf{h}}_{k,M_k(j)}^H \mathbf{h}_{k,M_k(j)}\right\}, \tag{19}$$

$$\mathbf{C}_{kk'} \in \mathbb{C}^{J \times J}, \\ c_{kk'}^{jj'} \triangleq \mathbb{E}\left\{\hat{\mathbf{h}}_{k,M_k(j)}^H \mathbf{h}_{k',M_k(j)} \mathbf{h}_{k',M_k(j')}^H \hat{\mathbf{h}}_{k,M_k(j')}\right\}, \tag{20}$$

$$\mathbf{D}_k \in \mathbb{C}^{J \times J}, \\ d_k^{jj} \triangleq \mathbb{E}\left\{\hat{\mathbf{h}}_{k,M_k(j)}^H \mathbf{n}_{M_k(j)} \mathbf{n}_{M_k(j)}^H \hat{\mathbf{h}}_{k,M_k(j)}\right\}, \tag{21}$$

where w_k^j and b_k^j are the jth elements of $\mathbf{w}_k$ and $\mathbf{b}_k$, respectively. $c_{kk'}^{jj'}$ is the element in the jth row and j'th column of $\mathbf{C}_{kk'}$. $\mathbf{D}_k$ is a diagonal matrix. Furthermore, the known $\left\{\bar{\mathbf{h}}_{k,m}\right\}$ and $\{\beta_{k,m}\}$ are used, and the above elements can be rewritten as

$$b_k^j = \tau_p p_p \left(\bar{\mathbf{h}}_{k,M_k(j)}^H \boldsymbol{\Phi}_{k,M_k(j)}^{-1} \mathbf{R}_{k,M_k(j)} \bar{\mathbf{h}}_{k,M_k(j)} + \beta_{k,M_k(j)} \mathrm{tr}\left(\boldsymbol{\Phi}_{k,M_k(j)}^{-1} \mathbf{R}_{k,M_k(j)}\right)\right), \tag{22}$$

$$d_k^{jj} = \sigma^2 \mathrm{tr}\left(\hat{\mathbf{R}}_{k,M_k(j)}\right). \tag{23}$$

The diagonal elements and other elements of $\mathbf{C}_{kk'}$ are respectively expressed as (24) and (25) shown at the top of the next page, where $\mathrm{Re}\{\cdot\}$ represents the real part. $\mathrm{I}_{\mathcal{P}(k)}(k')$ is set as the indicator function, namely

$$\mathrm{I}_{\mathcal{P}(k)}(k') = \begin{cases} 1, & \text{if} \quad k' \in \mathcal{P}(k) \\ 0, & \text{if} \quad k' \notin \mathcal{P}(k) \end{cases}. \tag{26}$$

Then (17) can be rewritten as

$$SINR_k = \frac{\eta_k \left|\mathbf{w}_k^H \mathbf{b}_k\right|^2}{\mathbf{w}_k^H \left(\sum\limits_{k'=1}^{K} \eta_{k'} \mathbf{C}_{k,k'} - \eta_k \mathbf{b}_k \mathbf{b}_k^H + \mathbf{D}_k\right) \mathbf{w}_k}. \tag{27}$$

The uplink rate that IR k can achieve is

$$R_k = \frac{\tau_u}{\tau_c} B \log_2\left(1 + SINR_k\right). \tag{28}$$

IV. AP Selection and Pilot Assignment

A. AP selection

Since each IR is only served by J APs from G_{sub} APGs, each IR has to select the APs which can provide the best services for it. A LoS path gain based AP selection method is proposed, as shown in Algorithm 1. Our goal is to select the APs with the best channel conditions to provide services in units of APG. When selecting the serving APs for IR k, the MAP in each APG calculates the sum of the LoS path gain between IR k and all APs in this APG, namely

$$\alpha_{k,g}^{sum} = \sum_{m \in \mathcal{A}(g)} \alpha_{k,m}, g = 1, \cdots, G. \tag{29}$$

Then the set $\left\{\alpha_{k,g}^{sum}\right\}$ can be obtained. The elements in this set are sorted from largest to smallest, and the APGs corresponding to the first G_{sub} items are selected to serve IR k.

$$c_{kk'}^{jj} = \mathrm{tr}\left(\hat{\mathbf{R}}_{k,M_k(j)}\mathbf{R}_{k',M_k(j)}\right) + \mathrm{I}_{\mathcal{P}(k)}\left(k'\right)\tau_p^2 p_p^2 \beta_{k',M_k(j)} \times \left(2\mathrm{Re}\left\{\bar{\mathbf{h}}_{k',M_k(j)}^H \mathbf{\Phi}_{k,M_k(j)}^{-1}\mathbf{R}_{k,M_k(j)}\bar{\mathbf{h}}_{k',M_k(j)}\mathrm{tr}\left(\mathbf{R}_{k,M_k(j)}\mathbf{\Phi}_{k,M_k(j)}^{-1}\right)\right\} + \beta_{k',M_k(j)}\left|\mathrm{tr}\left(\mathbf{\Phi}_{k,M_k(j)}^{-1}\mathbf{R}_{k,M_k(j)}\right)\right|^2\right), \quad (24)$$

$$c_{kk'}^{jj'} = \mathrm{I}_{\mathcal{P}(k)}\left(k'\right)\tau_p^2 p_p^2 \left(\bar{\mathbf{h}}_{k',M_k(j)}^H \mathbf{\Phi}_{k,M_k(j)}^{-1}\mathbf{R}_{k,M_k(j)}\bar{\mathbf{h}}_{k',M_k(j)} + \beta_{k',M_k(j)}\mathrm{tr}\left(\mathbf{\Phi}_{k,M_k(j)}^{-1}\mathbf{R}_{k,M_k(j)}\right)\right) \times \left(\bar{\mathbf{h}}_{k',M_k(j')}^H \mathbf{\Phi}_{k,M_k(j')}^{-1}\mathbf{R}_{k,M_k(j')}\bar{\mathbf{h}}_{k',M_k(j')} + \beta_{k',M_k(j')}\mathrm{tr}\left(\mathbf{\Phi}_{k,M_k(j')}^{-1}\mathbf{R}_{k,M_k(j')}\right)\right)^*, j \neq j' \quad (25)$$

Additionally, the LSF coefficient $\beta_{k,m}$ or the distance $d_{k,m}$ between AP m and IR k can be selected instead of $\alpha_{k,m}$. When distance $d_{k,m}$ is used as the metric, the sorting method in step 5 in Algorithm 1 should be changed to sort from smallest to largest. The system performance under the three methods is compared in the simulations.

The quicksort algorithm is used to perform the sorting operations in Algorithm 1, then the complexity of the proposed AP selection algorithm is $O\left(K\left(G + G\log G\right)\right)$. If the serving APs are directly selected for each IR instead of the serving APGs, the complexity of this operation is $O\left(K\left(M\log M\right)\right)$, which is higher because $M \gg G$. If there is no special declaration, the sorting operations in all the algorithms below are also quicksort.

Algorithm 1 AP Selection Algorithm

Input: LoS path gain set $\{\alpha_{k,m}\}$.
for $k = 1$ to K **do**
  The MAP in each APG calculates the sum of the LoS path gain between IR k and all APs in this APG;
  The set $\left\{\alpha_{k,g}^{sum}\right\}$ is obtained where $g = 1, \cdots, G$;
  Sort all elements in $\left\{\alpha_{k,g}^{sum}\right\}$ from largest to smallest;
  Select the APGs corresponding to the first G_{sub} items to serve IR k, namely $\mathcal{G}(k)$;
  Select the APs in these APGs to constitute the set $\mathcal{M}(k)$;
end for
Output: Serving AP set $\mathcal{M}(k)$ for $k = 1, 2, \cdots K$.

B. Pilot Assignment

There are τ_p mutually orthogonal pilots used for channel estimation, and $\tau_p < K$. To reduce the interference of pilot signals from different IRs, thereby ensuring the accuracy of channel estimation, it is necessary to design a suitable pilot assignment scheme. To make full use of pilot resources and simplify the analysis, it is assumed that the number of IRs assigned each pilot is equal, which is $K_p = K/\tau_p$. Then, we propose an IR location based pilot assignment scheme by improving the method of selecting the initial cluster heads in the K-Means++ [2]. In the K-Means++ algorithm, several points as dispersed as possible are selected as the initial cluster centers. The principle of pilot assignment is also to select the IRs with the distribution as dispersed as possible to use the same pilot.

Algorithm 2 IR Location based Pilot Assignment Scheme

Initialize: The set $\mathcal{R}$ of all IRs; the set $\mathcal{R}_i$ of IRs assigned the ith pilot. Set $\mathcal{R}_i = \emptyset$ for $i = 1, \cdots, \tau_p$.

1) Determine the initial IR set $\mathcal{R}_0$

Calculate the distance d_k from IR k to the center of the area for $k = 1, 2, \cdots, K$;
Sort all elements in $\{d_k\}$ from smallest to largest, then select the IRs corresponding to the first τ_p items to constitute the initial IR set $\mathcal{R}_0$;
Remove the IRs belonging to $\mathcal{R}_0$ from $\mathcal{R}$;

2) Pilot Assignment

for $i = 1$ to $\tau_p - 1$ **do**
  Select the ith IR from $\mathcal{R}_0$ as the first IR using the ith pilot, and add it into $\mathcal{R}_i$;
  Remove the IR from $\mathcal{R}$;
  repeat
    For each IR in $\mathcal{R}$, calculate the distance between it and all IRs in $\mathcal{R}_i$, and denote the smallest distance as $d_k^{\min}$;
    Sort all elements in $\left\{d_k^{\min}\right\}$ from largest to smallest, then select the IR corresponding to the λth item as the next IR using the ith pilot;
    Add the IR into $\mathcal{R}_i$ and remove it from $\mathcal{R}$;
  until the K_p IRs using the ith pilot are determined;
end for
All remaining IRs constitute the set $\mathcal{R}_{\tau_p}$;

Output: The set $\mathcal{R}_i$ for $i = 1, \cdots, \tau_p$.

As shown in Algorithm 2, the pilot assignment scheme mainly includes two steps: determining the initial IR set $\mathcal{R}_0$ and assigning pilots. Let i denote the index of the ith pilot where $i \in \{1, \cdots, \tau_p\}$, and the indexes of the pilots are the order in which the pilots are assigned. Next, the purpose of the first step in Algorithm 2 is explained. If the first IR using the ith pilot is selected randomly, the distribution of the K_p IRs assigned the ith pilot may be related to the value of i. In other words, if some pilot is assigned first, the distribution of IRs using this pilot will be more dispersed. But if some pilot is assigned last, the IRs using the pilot may be concentrated in the center of the area. Determining the set $\mathcal{R}_0$ can ensure that the τ_p IRs closest to the center of the area are assigned different pilots, avoiding the occurrence of the above-mentioned situation.

If $\lambda = 1$ in the second step of Algorithm 2, the distribution

of IRs using the pilots which are assigned last may be not enough dispersed, especially the τ_pth pilot. It can avoid the occurrence of the above-mentioned situation to set an appropriate value for λ, and $\lambda < K_p$. The system performance under the pilot assignment scheme with different λ values is shown in the simulations.

The complexity of the K-Means based pilot assignment scheme in [18] is $O(TK)$, where T is the number of iterations. In Algorithm 2, the complexity of the stage of determining the initial IR set is $O(K \log K)$, and the complexity of assigning pilots is $O\left(K^2 + K \log K\right) = O\left(K^2\right)$, which is independent of the number of iterations. The system performance under these two pilot assignment schemes is compared in the simulations.

V. Power Control and Backhaul Combining

The goal of CFmMIMO is to provide uniform QoS to all users, so it is the optimization objective to maximize the minimum rate by power control. Moreover, the high reliability of signal transmission is a very important performance metric in indoor industrial scenarios. Maximizing the minimum SINR can better meet high reliability [27]. Therefore, the objective function to be solved is

$$\begin{aligned} &\max_{\{\eta_k\},\{\mathbf{w}_k\}} \min_{k=1,\cdots,K} SINR_k \\ &s.t.\ C1: 0 \le \eta_k \le p_u, k = 1, \cdots, K \\ &\quad\ C2: \left\|\mathbf{w}_k\right\| \le 1, k = 1, \cdots, K \end{aligned}, \tag{30}$$

where $\{\eta_k\}$ and $\{\mathbf{w}_k\}$ are the sets of power control coefficients and backhaul combining coefficient vectors for $k = 1, 2, \cdots K$. $C1$ indicates that the maximum transmit power of each IR is p_u. $C2$ is the constraint on the backhaul combining coefficients. After auxiliary variable t is introduced, (30) can be equivalently rewritten into the following form:

$$\begin{aligned} &\max_{\{\eta_k\},\{\mathbf{w}_k\},t} t \\ &s.t.\ C1: 0 \le \eta_k \le p_u, k = 1, \cdots, K \\ &\quad\ C2: \left\|\mathbf{w}_k\right\| \le 1, k = 1, \cdots, K \\ &\quad\ C3: t \le SINR_k, k = 1, \cdots, K \end{aligned}. \tag{31}$$

In the case that $\{\mathbf{w}_k\}$ is given, problem (31) is quasi-linear and can be solved by bisection method. When $\{\eta_k\}$ is given, the expression of $SINR_k$ is a generalized Rayleigh quotient for $k = 1, 2, \cdots K$, so the method in [31] can be used to obtain the optimal $\{\mathbf{w}_k\}$. Therefore, the problem (31) can be solved alternately in terms of $\{\eta_k\}$ and $\{\mathbf{w}_k\}$, as shown in Algorithm 3.

Algorithm 3 is an improvement to the bisection method. The objective function in problem (32) is to minimize the sum of power control coefficients, namely $\sum_{k=1}^{K} \eta_k$. The purpose is to select one of all feasible solutions to continue the following steps. Since the SINR of each IR will increase after the backhaul combining, and there may be t larger than $t_{\max}$ in the previous iteration that satisfying the constraints in (32). Therefore, in each iteration of Algorithm 3, if the problem (32) is feasible, the bisection interval needs to be dynamically adjusted [30], which is different from the traditional bisection method.

In step 4 of Algorithm 3, the CVX is used to solve the convex problem, and the complexity of this operation is $O\left(K^{3.5} \log\left(1/\varepsilon\right)\right)$ [32], where ε is the precision of the CVX solution. The complexity of calculating the backhaul combining coefficients in step 7 is $O(K)$. Let T denote the number of iterations in Algorithm 3, then the complexity of the proposed joint optimization algorithm can be expressed as $O\left(T\left(K^{3.5} \log\left(1/\varepsilon\right) + K\right)\right)$. If the process of optimizing the backhaul combining is ignored, the complexity of Algorithm 3 is the same as that of the bisection in [1]. The system performance under these different algorithms is compared in the simulations.

Algorithm 3 Joint Optimization Algorithm for Power Control and Backhaul Combining

1: **Initialize:** Set appropriate initial values for $t_{\min}$ and $t_{\max}$. Initialize backhaul combining vector set $\{\mathbf{w}_k\}$. Set appropriate values for δ and γ, where $\delta > 0$ and $\gamma > 1$.
2: **while** $t_{\max} - t_{\min} > \delta$ **do**
3: set $t = \frac{t_{\max} + t_{\min}}{2}$;
4: when $\{\mathbf{w}_k\}$ and t are given, solve the following convex problem:

$$\begin{aligned} &\min_{\{\eta_k\}} \sum_{k=1}^{K} \eta_k \\ &s.t.\ C1: 0 \le \eta_k \le p_u, k = 1, \cdots, K \\ &\quad\ C2: \left(1+t\right)\eta_k \left|\mathbf{w}_k^H \mathbf{b}_k\right|^2 - t \sum_{i=1}^{K} \eta_i \mathbf{w}_k^H \mathbf{C}_{ki} \mathbf{w}_k \\ &\qquad - t \mathbf{w}_k^H \mathbf{D}_k \mathbf{w}_k \ge 0, k = 1, \cdots, K \end{aligned}; \tag{32}$$

5: **if** (32) is feasible **then**
6: Set the solution $\{\tilde{\eta}_k\}$ of problem (32) as power control coefficients $\{\eta_k\}$;
7: When $\{\eta_k\}$ is given, update $\{\mathbf{w}_k\}$ according to (33) and (34):

$$\mathbf{w}_k = \left(\sum_{i=1}^{K} \eta_i \mathbf{C}_{k,i} - \eta_k \mathbf{b}_k \mathbf{b}_k^H + \mathbf{D}_k\right)^{-1} \sqrt{\eta_k} \mathbf{b}_k; \tag{33}$$

$$\tilde{\mathbf{w}}_k = \frac{\mathbf{w}_k}{\left\|\mathbf{w}_k\right\|}; \tag{34}$$

8: Use $\{\tilde{\eta}_k\}$ and $\{\tilde{\mathbf{w}}_k\}$ to calculate the SINR of each IR, and set $\tilde{t}$ as the minimum of these SINRs;
9: Set $t_{\min} = \tilde{t}$ and $t_{\max} = \gamma \tilde{t}$;
10: **else**
11: Set $t_{\max} = t$;
12: **end if**
13: **end while**
14: **Output:** Optimal power control coefficient set $\left\{\eta_k^{opt}\right\}$, optimal backhaul combining vector set $\left\{\mathbf{w}_k^{opt}\right\}$.

VI. System Scalability

The scalability of the CFmMIMO system means that when the network scale (number of APs) and network load (number of users) continue to increase, the capacity of the backhaul links and the computing capabilities of APs and CPUs can always meet the demand [6], [23]. Specifically, the backhaul link capacity needs to meet data transmission and CSI sharing, and the computing capabilities of APs and CPUs need to meet channel estimation, signal processing, and power control [23]. In indoor industrial scenarios, especially when there are many access devices, network scalability is an issue that must be considered.

A. Scalability Analysis

The analysis for the scalability of the proposed CFmMIMO system are as follows:

- *Network topology:* In the canonical CFmMIMO architecture, each AP is directly connected to the CPU, which will consume a lot of cables and cause high CPU load, so this topology is not easy to be practically deployed in industrial scenarios. The proposed hierarchical network topology based on AP grouping is easier to deploy and more scalable.
- *AP selection:* In the canonical CFmMIMO architecture, each user is served by all APs simultaneously, which is obviously unnecessary and not scalable [7], [8], [23]. In the cell-free network proposed in this paper, each IR is only served by the APs with the best channel conditions, which means that each AP only needs to serve a small subset of the IRs, which greatly enhances the scalability of the network. In addition, the AP selection method proposed in this paper selects APGs for each AP instead of directly selecting the serving APs, making the computational load on the CPU be reduced, so it is more scalable.
- *Pilot assignment:* The proposed pilot assignment scheme is performed jointly for all IRs, but only the location information of the IRs is needed. Therefore, a special processing unit can be set up to perform the computing task of pilot assignment.
- *Channel estimation:* Each AP only needs to serve a small subset of the IRs, so each AP only needs to estimate the channel state between it and the served IRs. Therefore, the computational load on the APs is reduced and scalability of the network is enhanced.
- *Backhaul link capacity:* Each AP only needs to upload data from the IRs it serves to the CPU, and the proposed CFmMIMO system does not require CSI sharing. Therefore, the requirement for backhaul link capacity is reduced.
- *Power control:* The proposed power control method is network-wide power control, which requires the CPU to jointly control the power of all IRs. In addition, multiple iterations are required to solve the power control problem. The computational complexity of power control will continue to increase when the number of IRs increases.
- *Backhaul combining:* Given the power control coefficients, the backhaul combining coefficients can be obtained by a closed-form solution, which only depends on the knowledge of channel statistics. It can be reasonably assumed that the computing capabilities of the CPU can meet the demand.

B. Scalable Power Control

From the above analysis, it can be seen that the power control problem is the most difficult to meet scalability requirement. The canonical power control methods are network-wide power control, which jointly optimizes the transmit power of all users. There may also be the "butterfly effect" caused by inaccurate channel estimation [8]. There is a distributed uplink power control method in [6], where the transmit power of each user is controlled separately. If the LoS path gain $\{\alpha_{k,m}\}$ is used as the metric, the transmit power of IR k is given by

$$\eta_k = p_u \frac{\left(\sum\limits_{m\in\mathcal{M}(k)} \alpha_{k,m}\right)^{-\frac{1}{2}}}{\max\limits_{k'\in\{1,\cdots,K\}} \left(\sum\limits_{m\in\mathcal{M}(k')} \alpha_{k',m}\right)^{-\frac{1}{2}}}. \tag{35}$$

The above-mentioned distributed power control method still aims at fairness, that is, the IRs with poor channel conditions have higher transmit power. However, the denominator in (35) needs to calculate the maximum value among the K terms, so its scalability still needs to be enhanced. Therefore, a scalable power control method is proposed below.

Taking the total path gain of each APG mentioned in Section IV as the metric, namely $\left\{\alpha_{k,g}^{sum}\right\}$, each IR selects the APG with the best channel condition among the APGs serving it, and the corresponding MAP performs power control for it. The set of IRs associated with the gth MAP is denoted by $\mathcal{S}(g)$. If $k \in \mathcal{S}(g)$, the transmit power of IR k is given by

$$\eta_k = p_u \frac{\left(\alpha_{k,g}^{sum}\right)^{-\frac{1}{2}}}{\max\limits_{k'\in\mathcal{S}(g)} \left(\alpha_{k',g}^{sum}\right)^{-\frac{1}{2}}}. \tag{36}$$

The number of IRs in $\mathcal{S}(g)$ is much smaller than K, so the scalability of power control is further enhanced. In the simulations, the system performance under the above two power control methods is compared.

VII. Simulations and Discussions

In the simulations, an indoor industrial workshop with a squre area of 200 m $\times$ 200 m and a height of 5 m is considered. All APs are uniformly deployed on the top of the workshop. Unless otherwise specified, the parameters in the simulations are set as follows. The number of APs is $M = 64$, and each AP is equipped with $N = 4$ antennas [27]. The bandwidth of

This article has been accepted for publication in IEEE Transactions on Communications. This is the author's version which has not been fully edited and content may change prior to final publication. Citation information: DOI 10.1109/TCOMM.2022.3210410

the system is 100 MHz [27]. All APs are divided into sixteen APGs, namely $G = 16$. Each IR is served by the APs in four APGs, namely $G_{sub} = 4$ and $J = 16$. The number of IRs is $K = 40$, and all IRs are uniformly distributed at random in the workshop [1]. The carrier frequency selected in the simulations is 3.4 GHz, and the indoor hotspot channel model in [30] is adopted. The number of samples in each coherence interval is $\tau_c = 200$, where $\tau_p = 5$ and $\tau_u = 160$. The maximum transmit power of each IR is $p_u = 0.2$ W, and the pilot transmit power is $p_p = 0.2$ W. Finally, the variance of the noise is $\sigma^2 = -96$ dBm.

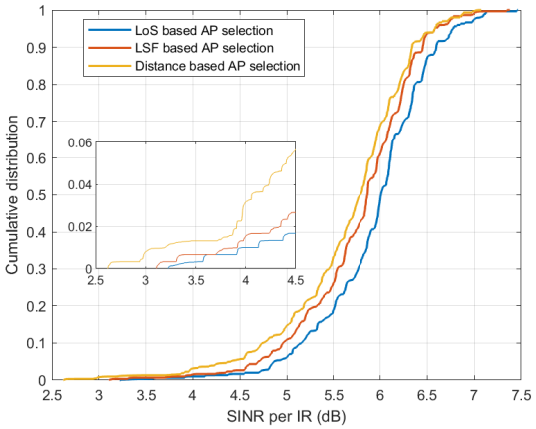

Fig. 2. Comparison of three AP selection methods.

Firstly, the system performance under the three AP selection methods is compared, as shown in Fig. 2. 300 random realizations of IRs distribution and channel state are generated. In other simulations, if there is no special statement, the number of realizations is also 300. In each realization, the SINR per IR under the three AP selection methods is obtained. Therefore, each curve represents the cumulative distribution function (CDF) of $300 \times K = 12000$ values. The leftmost point of each curve represents the lowest SINR, and the rightmost point represents the highest SINR. It can be seen from Fig. 2 that the system performance under the three AP selection methods is very close. However, the blue curve is overall on the right side of the other two curves, indicating the SINR under the AP selection method based on LoS path gain is a little higher, so this AP selection method is used in the following simulations.

Fig. 3 shows the distribution of IRs after the proposed pilot assignment scheme is applied, and the dots with the same color represent the IRs using the same pilot. Fig. 3(a) and Fig. 3(b) correspond to the cases with $\lambda = 1$ and $\lambda = 5$ respectively, where the black triangles represent the IRs assigned the τ_pth pilot, namely the last pilot assigned. It can be seen that the distribution of the black triangles in Fig. 3(b) is more dispersed than that in Fig. 3(a), that is, the pilot reuse distances are longer. In Fig. 4, these two cases are compared numerically in terms of the CDF of SINR per IR. Obviously, when $\lambda = 5$, the system performance under the proposed scheme is better than when $\lambda = 1$. Especially for the smallest SINR metric, the former is about 25% larger than the latter. The reason

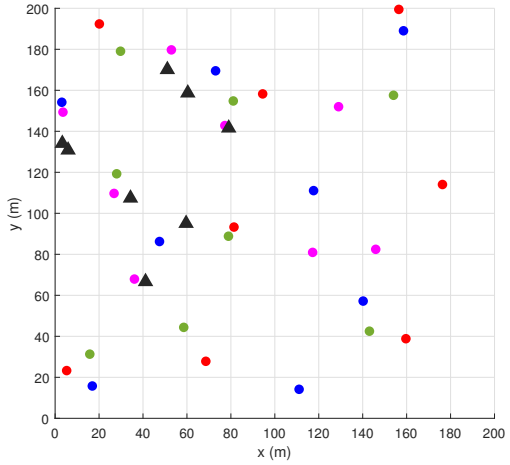

(a) $\lambda = 1$

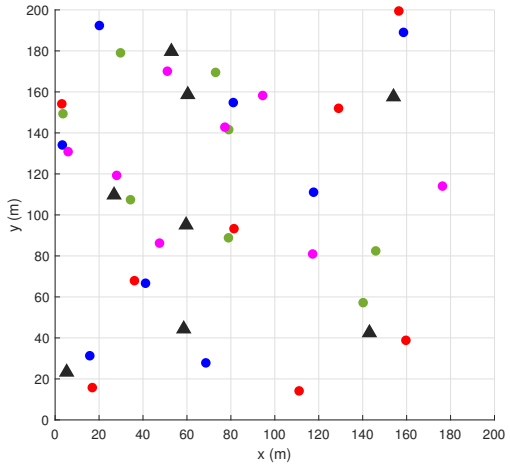

(b) $\lambda = 5$

Fig. 3. The IR distribution after the proposed pilot assignment scheme is applied.

is that the black triangles in Fig. 3(a) are denser, then pilot contamination leads to lower channel estimation accuracy and affects the achievable SINR. In addition, the proposed pilot assignment scheme is compared with the K-Means based pilot assignment scheme in [18]. The yellow curve in Fig. 4 is completely on the right side of the blue curve, indicating that the proposed scheme is obviously better than the compared K-Means based pilot assignment scheme.

Fig. 5 shows the convergence of the proposed power control and backhaul combining algorithm under different parameter settings. As can be seen from Fig. 5, when the algorithm converges, the average rate the system can achieve under $\delta = 0.01$ is higher than that under $\delta = 0.1$. In both cases, the algorithm converges faster when $\gamma = 2$ than when $\gamma = 3$. Obviously, the value of δ will determine whether the optimal solution can be obtained, and the value of γ will affect the convergence speed of the algorithm. When $\delta = 0.01$ and $\delta = 0.001$, the convergence of the algorithm is almost the same, and the average rate that the system can achieve when the algorithm converges is also the same, indicating that

when δ is 0.01 or less, the optimal solution can be obtained. Therefore, in the simulations in this paper, the δ and γ are set to 0.01 and 2, respectively, which can achieve highest average rate and converge faster.

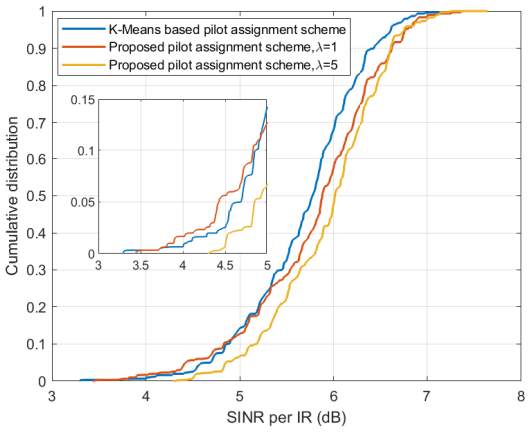

Fig. 4. Comparison of different pilot assignment schemes.

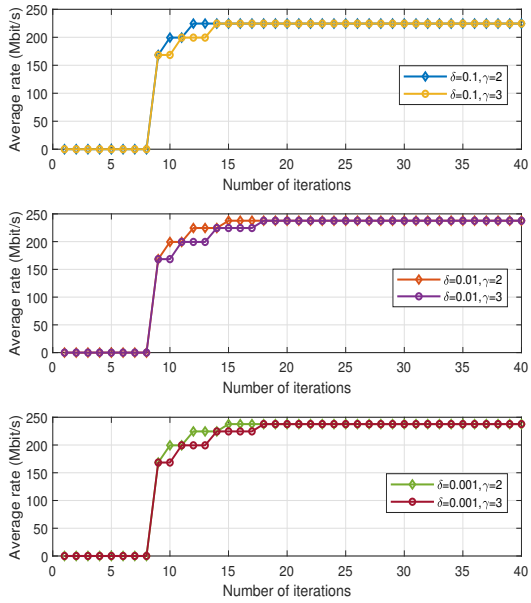

Fig. 5. Convergence of the proposed power control and backhaul combining joint optimization algorithm under different parameter settings.

Next, the effectiveness of the proposed joint optimization algorithm for power control and backhaul combining is demonstrated and analyzed. The bisection based power control (BPC) method in [1] is combined with equal gain combining (EGC) [21] and optimal backhaul combining (OBC) proposed in this paper to form algorithms BPC-EGC and BPC-OBC, respectively. Fig. 6 shows the system performance under the three algorithms. As can be seen from Fig. 6(a), the lowest SINR under BPC-EGC and BPC-OBC is about 0 dB, but overall the latter can achieve better performance than the

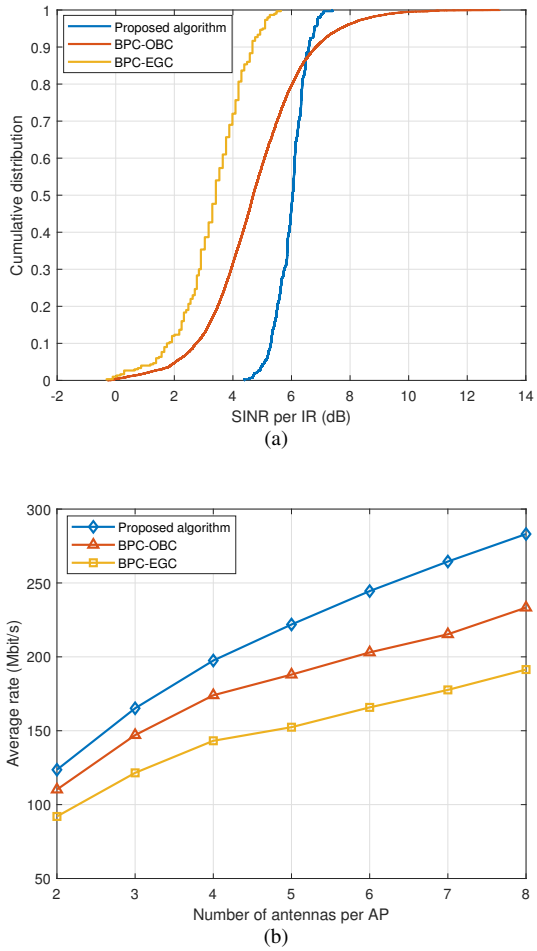

Fig. 6. Comparison of system performance under different power control algorithms: a. The CDF of uplink SINR per IR; b. Average uplink rate versus the number of antennas per AP.

former. The lowest SINR under the proposed algorithm is about 4 dB, which is much higher than that under the other two algorithms. It is obvious that the proposed algorithm can enable all IRs to obtain higher SINR and better ensure the fairness of QoS, which is the goal of cell-free networks. Fig. 6(b) shows that the average uplink rate of the system under the proposed algorithm is significantly higher than that under the other two algorithms. And as the number of antennas increases, the rate gap becomes larger.

Fig. 7(a) shows the CDF of SINR per IR for different network scales (the number of APs) in the proposed scenario. The three cases of $M = 36$, $M = 64$, and $M = 100$ are set, indicating that the distribution of APs is becoming denser. The corresponding number of APGs are $G = 9$, $G = 16$, and $G = 25$ in order. However, the number of APs serving each IR is fixed in the three cases. Obviously, when APs are more densely deployed, the SINR that IRs can achieve will be higher. The reason is that the J APs serving each IR will be closer to the IR, so the channel conditions will be better. Additionally, it can be seen from Fig. 7(b) that when the network scale is larger, the average uplink rate of the system is also higher, and it gets higher as the number of antennas

This article has been accepted for publication in IEEE Transactions on Communications. This is the author's version which has not been fully edited and content may change prior to final publication. Citation information: DOI 10.1109/TCOMM.2022.3210410

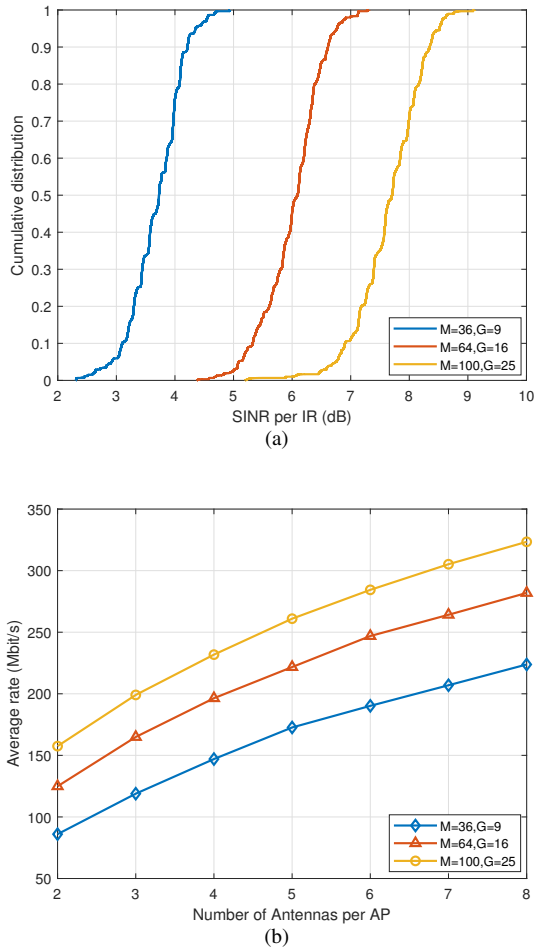

Fig. 7. Comparison of system performance under different network scales: a. The CDF of uplink SINR per IR; b. Average uplink rate versus the number of antennas per AP.

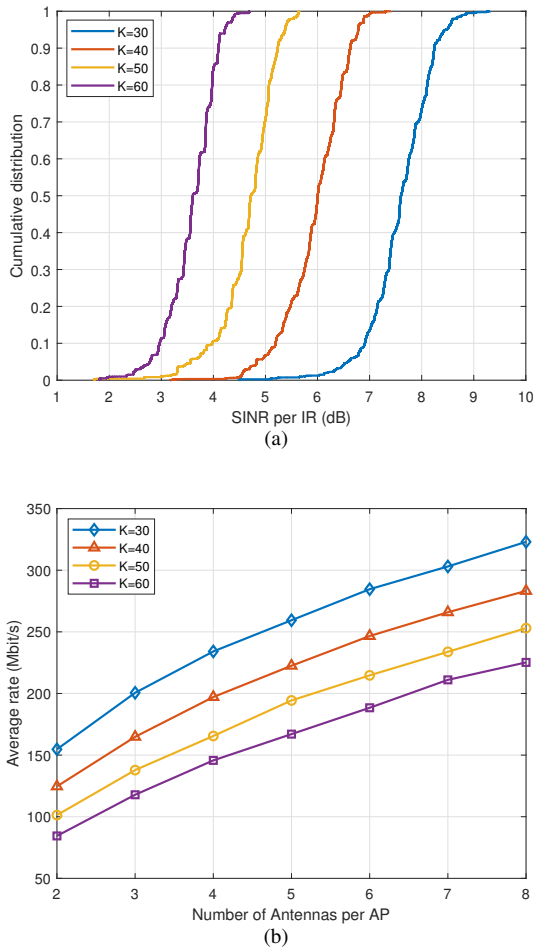

Fig. 8. Comparison of system performance under different network loads: a. The CDF of uplink SINR per IR; b. Average uplink rate versus the number of antennas per AP.

increases.

Fig. 8(a) shows the CDF of SINR per IR for different network loads (the number of IRs). The four cases of $K = 30$, $K = 40$, $K = 50$, and $K = 60$ are set. In order to make the number of SINR values included in each curve equal, the corresponding realization times of the four cases are 400, 300, 240 and 200 in order. Obviously, when the number of IRs is smaller, the SINR that IRs can achieve will be higher. The reason is that the distribution of IRs will be more dispersed, and the mutual interference among IRs will be weaker. Additionally, it can be seen from Fig. 8(b) that when the network load is less, the average uplink rate of the system is higher, and it gets higher as the number of antennas increases.

In Fig. 9, the effectiveness of the proposed scalable power control method is demonstrated and analyzed. The system performance under the proposed scalable power control method is almost the same as that under the distributed power control method in [6], but the former is more scalable than the latter. Compared with the network-wide max-min fairness power control method, the gap between the highest SINR and the lowest SINR under the other two methods is larger, indicating scalability is traded at the cost of fairness. The lowest SINR under the network-wide max-min fairness power control is about 3.4 dB, which is roughly equal to the 95%-likely SINR per IR under the scalable power control method. Therefore, when a small number of users in some industrial scenarios do not have strong requirement for high SINR, the proposed scalable power control method can still be used.

VIII. Conclusion

This paper studied the CFmMIMO system for indoor industrial scenarios. An easy-to-deploy hierarchical network topology based on AP grouping was proposed. Based on this, we proposed an effective AP selection method. Considering the pilot contamination, a pilot assignment scheme based on IR location was proposed. Considering the high reliability requirement of industrial data transmission, the power control and backhaul combining were jointly optimized with the objective of maximizing the minimum SINR. The scalability of the proposed CFmMIMO system was analyzed, and a scalable power control method was proposed. The simulations demonstrated that the proposed AP selection method, pilot assignment scheme, and the joint optimization algorithm for

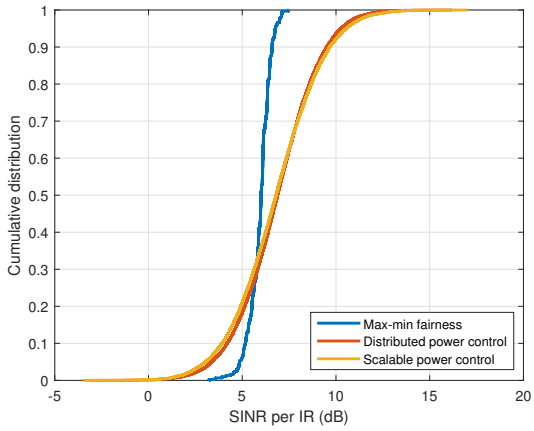

Fig. 9. Comparison of three power control methods.

power control and backhaul combining can effectively enhance the performance of the CFmMIMO system. Finally, the impact of network scale and network load on system performance was evaluated and analyzed in the simulations.

REFERENCES

[1] H. Q. Ngo, A. Ashikhmin, H. Yang, E. G. Larsson, and T. L. Marzetta, "Cell-free massive MIMO versus small cells," *IEEE Trans. Wirel. Commun.*, vol. 16, no. 3, pp. 1834–1850, Mar. 2017.

[2] H. Zhang, H. Zhang, W. Liu, K. Long, J. Dong, and V. C. M. Leung, "Energy efficient user clustering, hybrid precoding and power optimization in terahertz MIMO-NOMA systems," *IEEE J. Sel. Areas Commun.*, vol. 38, no. 9, pp. 2074–2085, Sept. 2020.

[3] H. Ma, H. Zhang, X. Wang, and J. Cheng, "Backhaul-aware user association and resource allocation for massive MIMO-enabled HetNets," *IEEE Commun. Lett.*, vol. 21, no. 12, pp. 2710–2713, Dec. 2017.

[4] T. Lu, H. Zhang, and K. long, "Joint beamforming and power control for MIMO-NOMA with deep reinforcement learning," in *Proc. IEEE Int. Conf. Commun. (ICC)*, Jun. 2021, pp. 1–5.

[5] L. Dai, "An uplink capacity analysis of the distributed antenna system (DAS): From cellular DAS to DAS with virtual cells," *IEEE Trans. Wirel. Commun.*, vol. 13, no. 5, pp. 2717–2731, May 2014.

[6] Ö. T. Demir, E. Björnson, and L. Sanguinetti, "Foundations of user-centric cell-free massive MIMO", *Foundations and Trends in Signal Processing*, vol. 14, no. 3–4, pp. 162–472.

[7] S. Buzzi and C. D'Andrea, "Cell-free massive MIMO: User-centric approach," *IEEE Wireless Commun. Lett.*, vol. 6, no. 6, pp. 706–709, Dec. 2017.

[8] G. Interdonato, P. Frenger, and E. G. Larsson, "Scalability aspects of cell-free massive MIMO," in *Proc. IEEE Int. Conf. Commun. (ICC)*, May 2019, pp. 1–6.

[9] H. Q. Ngo, L. Tran, T. Q. Duong, M. Matthaiou, and E. G. Larsson, "On the total energy efficiency of cell-free massive MIMO," *IEEE Trans. Green Commun. Netw.*, vol. 2, no. 1, pp. 25–39, Mar. 2018.

[10] J. C. Guo, Q. Y. Yu, W. B. Sun, and W. X. Meng, "Robust efficient hybrid pre-coding scheme for mmWave cell-free and user-centric massive MIMO communications," *IEEE Trans. Wirel. Commun.*, vol. 20, no. 12, pp. 8006–8022, Dec. 2021.

[11] L. D. Nguyen, T. Q. Duong, H. Q. Ngo, and K. Tourki, "Energy efficiency in cell-free massive MIMO with zero-forcing precoding design," *IEEE Commun. Lett.*, vol. 21, no. 8, pp. 1871–1874, Aug. 2017.

[12] E. Nayebi, A. Ashikhmin, T. L. Marzetta, H. Yang, and B. D. Rao, "Precoding and power optimization in cell-free massive MIMO systems," *IEEE Trans. Wirel. Commun.*, vol. 16, no. 7, pp. 4445–4459, Jul. 2017.

[13] M. Attarifar, A. Abbasfar, and A. Lozano, "Modified conjugate beamforming for cell-free massive MIMO," *IEEE Wireless Commun. Lett.*, vol. 8, no. 2, pp. 616–619, Apr. 2019.

[14] C. M. Yetis, E. Björnson, and P. Giselsson, "Joint analog beam selection and digital beamforming in millimeter wave cell-free massive MIMO systems," *IEEE Open J. Commun. Soc.*, vol. 2, pp. 1647–1662, Jul. 2021.

[15] Y. Li and G. A. Aruma Baduge, "NOMA-aided cell-free massive MIMO systems," *IEEE Wireless Commun. Lett.*, vol. 7, no. 6, pp. 950–953, Dec. 2018.

[16] F. Guo, H. Lu, and Z. Gu, "Joint power and user grouping optimization in cell-free massive MIMO systems," *IEEE Trans. Wirel. Commun.*, vol. 21, no. 2, pp. 991–1006, Feb. 2022.

[17] J. Denis and M. Assaad, "Improving cell-free massive MIMO networks performance: A user scheduling approach," *IEEE Trans. Wirel. Commun.*, vol. 20, no. 11, pp. 7360–7374, Nov. 2021.

[18] M. Attarifar, A. Abbasfar, and A. Lozano, "Random vs structured pilot assignment in cell-free massive MIMO wireless networks," in *Proc. IEEE Int. Conf. Commun. Workshops*, May 2018, pp. 1–6.

[19] W. Zeng, Y. He, B. Li, and S. Wang, "Pilot assignment for cell free massive MIMO systems using a weighted graphic framework," *IEEE Trans. Veh. Technol.*, vol. 70, no. 6, pp. 6190–6194, Jun. 2021.

[20] M. Guenach, A. A. Gorji, and A. Bourdoux, "Joint power control and access point scheduling in fronthaul-constrained uplink cell-free massive MIMO systems," *IEEE Trans. Commun.*, vol. 69, no. 4, pp. 2709–2722, Apr. 2021.

[21] T. K. Nguyen, H. H. Nguyen, and H. D. Tuan, "Max-min QoS power control in generalized cell-free massive MIMO-NOMA with optimal backhaul combining," *IEEE Trans. Veh. Technol.*, vol. 69, no. 10, pp. 10949–10964, Oct. 2020.

[22] X. Wang, A. Ashikhmin, Z. Dong, and C. Zhai, "Two-stage channel estimation approach for cell-free IoT with massive random access," *IEEE J. Sel. Areas Commun.*, vol. 40, no. 5, pp. 1428–1440, May 2022. 1678–1697, Aug. 2020.

[23] E. Björnson and L. Sanguinetti, "Scalable cell-free massive MIMO systems," *IEEE Trans. Commun.*, vol. 68, no. 7, pp. 4247–4261, Jul. 2020.

[24] W. Jiang, B. Han, M. A. Habibi, and H. D. Schotten, "The road towards 6G: A comprehensive survey," *IEEE Open J. Commun. Soc.*, vol. 2, pp. 334–366, Feb. 2021.

[25] A. Banchs, D. M. Gutierrez-Estevez, M. Fuentes, M. Boldi, and S. Provvedi, "A 5G mobile network architecture to support vertical industries," *IEEE Commun. Mag.*, vol. 57, no. 12, pp. 38–44, Dec. 2019.

[26] W. Nakimuli, J. Garcia-Reinoso, J. E. Sierra-Garcia, P. Serrano, and I. Q. Fernández, "Deployment and evaluation of an industry 4.0 use case over 5G," *IEEE Commun. Mag.*, vol. 59, no. 7, pp. 14–20, Jul. 2021.

[27] M. Alonzo, P. Baracca, S. R. Khosravirad, and S. Buzzi, "Cell-free and user-centric massive MIMO architectures for reliable communications in indoor factory environments," *IEEE Open J. Commun. Soc.*, vol. 2, pp. 1390–1404, Jun. 2021.

[28] X. Wang and C. Zhai, "Dynamic power control for cell-free Industrial Internet of Things with random data arrivals," *IEEE Trans. Industr. Inform.*, vol. 18, no. 6, pp. 4138–4147, Jun. 2022.

[29] H. Yan, A. Ashikhmin, and H. Yang, "Optimally supporting IoT with cell-free massive MIMO," in *Proc. IEEE Glob. Commun. Conf. (GLOBECOM)*, Dec. 2020, pp. 1–6.

[30] Ö. T. Demir and E. Björnson, "Joint power control and LSFD for wireless-powered cell-free massive MIMO," *IEEE Trans. Wirel. Commun.*, vol. 20, no. 3, pp. 1756–1769, Mar. 2021.

[31] Ö. Özdogan, E. Björnson, and J. Zhang, "Performance of cell-free massive MIMO with Rician fading and phase shifts," *IEEE Trans. Wirel. Commun.*, vol. 18, no. 11, pp. 5299–5315, Nov. 2019.

[32] T. Zhang, G. Liu, H. Zhang, W. Kang, J. Zhang, G. K. Karagiannidis, and A. Nallanathan, "Energy-efficient resource allocation and trajectory design for UAV relaying systems," *IEEE Trans. Commun.*, vol. 68, no. 10, pp. 6483–6498, Oct. 2020.

This article has been accepted for publication in IEEE Transactions on Communications. This is the author's version which has not been fully edited and content may change prior to final publication. Citation information: DOI 10.1109/TCOMM.2022.3210410

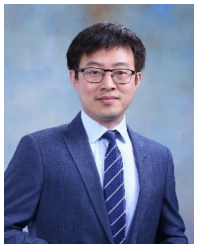

Haijun Zhang (Senior Member, IEEE) is currently a Full Professor and Associate Dean at University of Science and Technology Beijing, China. He was a Postdoctoral Research Fellow in Department of Electrical and Computer Engineering, the University of British Columbia (UBC), Canada. He serves/served as Track Co-Chair of WCNC 2020, Symposium Chair of Globecom'19, TPC Co-Chair of INFOCOM 2018 Workshop on Integrating Edge Computing, Caching, and Offloading in Next Generation Networks, and General Co-Chair of GameNets'16. He serves as an Editor of IEEE Transactions on Communications, IEEE Transactions on Network Science and Engineering, and IEEE Transactions on Vehicular Technology. He received the IEEE CSIM Technical Committee Best Journal Paper Award in 2018, IEEE ComSoc Young Author Best Paper Award in 2017, and IEEE ComSoc Asia-Pacific Best Young Researcher Award in 2019.

Renwei Su received the B.S. degree from the School of Computer and Communication Engineering, University of Science and Technology Beijing, China, in 2020, where he is currently pursuing the M.S. degree. His research interests include wireless communication, cell-free network, and massive MIMO.

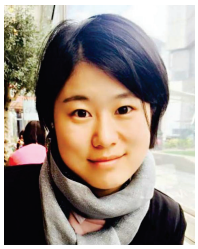

Yongxu Zhu (Senior Member, IEEE) received the Ph.D. degree in electrical engineering from University College London in 2017. From 2017 to 2019, she was a Research Associate with Loughborough University. She is currently a Senior Lecturer with the Division of Computer Science and Informatics, London South Bank University. Her research interests include wireless communication, heterogeneous networks, and physical-layer security. She has served as an Editor for the IEEE Wireless Communication Letters.

Keping Long (Senior Member, IEEE) received the M.S. and Ph.D. degrees from the University of Electronic Science and Technology of China, Chengdu, in 1995 and 1998, respectively. From September 1998 to August 2000, he was a Postdoctoral Research Fellow at the National Laboratory of Switching Technology and Telecommunication Networks, Beijing University of Posts and Telecommunications (BUPT), China. From September 2000 to June 2001, he was an Associate Professor at BUPT. From July 2001 to November 2002, he was a Research Fellow with the ARC Special Research Centre for Ultra Broadband Information Networks (CUBIN), University of Melbourne, Australia. He is currently a professor and Dean at the School of Computer and Communication Engineering, University of Science and Technology Beijing. He has published more than 200 papers, 20 keynote speeches, and invited talks at international and local conferences. His research interests are optical Internet technology, new generation network technology, wireless information networks, value-added services, and secure technology of networks. He was awarded by the National Science Fund for Distinguished Young Scholars of China in 2007 and selected as the Chang Jiang Scholars Program Professor of China in 2008. He is a member of the Editorial Committees of Sciences in China Series F and China Communications.

George K. Karagiannidis (Fellow, IEEE) was born in Pithagorion, Samos Island, Greece. He received the University Diploma (five years) and Ph.D. degrees in electrical and computer engineering from the University of Patras in 1987 and 1999, respectively. From 2000 to 2004, he was a Senior Researcher at the Institute for Space Applications and Remote Sensing, National Observatory of Athens, Greece. In June 2004, he joined the Faculty of the Aristotle University of Thessaloniki, Greece, where he is currently a Professor with the Electrical and Computer Engineering Department and the Head of the Wireless Communications and Information Processing (WCIP) Group. He is also an Honorary Professor at Southwest Jiaotong University, Chengdu, China. His research interests are in the broad area of digital communications systems and signal processing, with emphasis on wireless communications, optical wireless communications, wireless power transfer, and applications and communications and signal processing for biomedical engineering.,Dr. Karagiannidis has been involved as the general chair, the technical program chair, and a member of technical program committees in several IEEE and non-IEEE conferences. He is one of the highly-cited authors across all areas of electrical engineering, recognized from Clarivate Analytics as the Web of Science Highly-Cited Researcher in the six consecutive years 2015–2020. In the past, he was an editor in several IEEE journals. From 2012 to 2015, he was the Editor-in Chief of IEEE Communications Letters. He serves as the Associate Editor-in Chief for IEEE Open Journal of the Communications Society.